An adaptive machine vision system for full-field 3D surface profile measurement

H. N. Yen and D. M. Tsia
Machine Vision Lab.
Department of Industrial Engineering and Management
Yuan-Ze University, Chung-Li, Taiwan, R.O.C.
E-mail: iedmtsai@saturn.yzu.edu.tw

Abstract

3D surface profile measurement is important in manufacturing for process control and quality inspection. In this paper, a cost-effective machine vision system for adaptive and full-field 3D surface profiling applications is proposed. The system especially aims at the 3D inspection of small metallic objects that are the typical characteristics of electronic components such as weld solders and SMDs on PCBs. The proposed system is based on the phase shifting technique. A sinusoidal fringe pattern is projected on the object, and deformed in accordance with the object surface. The surface profile is obtained from the evaluation of intensity images of the deformed fringe patterns in different phase shifts. A software-controlled LCD panel is adopted to generate varying fringe patterns. It can shift the fringe pattern with accurate phase increments. During the phase shifting process it also eliminates vibration, which is the main error source in applying traditional phase shifting techniques. The system is adaptive because it can easily change the fringe period, phase-variation direction and projection area to accommodate the topography and reflectance of various objects. The measurement speed of the proposed system is fast. An image size of 640×480 pixels can be measured in less than 4 seconds with a typical personal computer. Experimental results from weld solders and SMT components on PCBs have shown the efficacy of the proposed method.

Keywords: Surface profile measurement; Fringe projection; Phase shift; 3D inspection

1. Introduction

Surface profile measurement is important in industrial inspection [1], and many nondestructive 3D profiling techniques [2-7] have been developed for the sake of product quality control and process efficiency. Recently, the trend toward miniaturization of electronic components and high-density packaging on circuit boards underscored the importance of 3D surface profile measurements in electronic manufacturing process to ensure the reliability of electronic devices.

Several nondestrctive techniques have been developed to measure the 3D surface profile of electronic components such as weld solders on print circuit boards (PCBs) and solder balls on ball grid arrays (BGAs). Laser scanning techniques [8-11] are popular in 3D inspection of solder paste and solder points. Tsukahera *et al*. [12] and Kim *et al*. [13] have developed laser vision systems to measure the surface height of solder bumps and solder balls on BGAs. However, their point-by-point or line-by-line scans are slow, and measuring accuracy is affected by beam spot reflection and stray light.

X-ray detection methods [14-17] are available for 3D measurements of electronic components such as solder joints on BGAs and flip chips. Nevertheless, they require expensive equipment and long measuring times. Microscope inspection with focus-based methods [18,19] has been applied to the shape measurement of solder joints on surface mounted devices (SMDs) and circuit boards with high accuracy. However, the inherently small effective area of microscope detection has limited its application for larger area inspections.

It can be seen that 3D surface profile measurement is increasingly important in electronic manufacturing. However, the aforementioned existing techniques are either slow, expensive or lack feasibility. A fast and cost-effective 3D surface profiling system is still needed in the electronic industry.

Among optical measuring methods, the projected fringes approaches [20,21] have been a full-field method for 3D measurement. Their measuring speed is fast and their implementation is simple. However, the measuring resolution of projected fringes methods is limited by the fringe density, and only points lying on the center-lines of fringes can be measured. Combined with phase shifting techniques [22], the measuring resolution of the projected fringes methods can be significantly improved and all points in the inspection area can be measured. This leads to the projected sinusoidal fringes with phase shifting techniques.

In the traditional projected sinusoidal fringes with phase shifting technique, the projected sinusoidal fringes pattern is acquired by the interference of two lasers, and the phase step is obtained by piezocrystal (PZT) [23]. Speckle noise produced by the laser interference affects measuring accuracy, and a strict optical setup environment is critical for successful measurement. PZT cannot accurately shift the phase step due to its nonlinear property and sensitivity to temperature and humidity and, therefore, the measuring accuracy is reduced.

The required sinusoidal fringe pattern in projected sinusoidal fringes with phase shifting technique can also be created by projecting an image of a white light illuminated sinusoidal transmission grating. Srinivasan *et al*. [24] used a defocused projection of a square wave-grating pattern to create the sinusoidal transmission

grating, and recorded the projection on a slide. A conventional slide projector was used to operate with the grating slide. The phase shifting was created by placing the slide projector on a stepper motor-driven translation stage. Their system is practical and no strict optical setup environment is needed, compared to the PZT method. However, the movement of a stepper motor-driven translation stage cannot be continuous and precise. Due to the mechanical movement of the translation stage, the accuracy of their measuring system is also affected by vibration, which is the main error source in applying phase shifting technique.

In this paper, we propose an adaptive, cost-effective 3D surface profile measuring system with LCD-based phase shifting technique and aim at the 3D inspection of small metallic objects found in the electronic industry. We adopt an LCD panel, and collocate with low cost optical components to create a fine fringe period of projected fringe pattern. The adopted LCD panel has uniform optical transparency and can be controlled by a personal computer. The unique electro-optical ability of the LCD panel makes it suitable for generating sinusoidal transmission gratings. Compared to the conventional phase shifting technique, the required sinusoidal fringe pattern can be created on an LCD panel and shifted accurately according to the desired phase increment by a software-controlled process instead of by physical movement of the slide projector. Measuring errors due to the mechanical movement of traditional methods for phase shifting can be eliminated in the proposed system. The proposed system can adaptively project fringe pattern with varying fringes period, phase-variation direction and projection area. Considering the different topographies and reflectances of various electronic products, adaptive projection is necessary to develop a 3D surface profiling system for the inspection of various small metallic electronic components.

This paper is organized as follows. Section 2 introduces the principle of the proposed method. Section 3 describes the layout, calibration and measurement procedure of the LCD-based 3D profiling system. Experimental results from standard 1 *mm*-gauge block, coin, weld solders and SMT components on PCBs are presented and analyzed in section 4. Section 5 concludes this paper.

2. Principle of 3D Measurement

2.1 Optical geometry

The optical geometry of the projected fringes method is shown in Figure 1. The optical axis of projection is normal to the reference plane, which coincides with the x-y plane. The surface height $h(x, y)$ of the object at coordinates (x, y) is evaluated with respect to the reference plane, and can be induced by the optical triangulation as

$$h(x, y) = \frac{P_o}{2\pi} \tan\theta_d \cdot [\phi_r(x, y) - \phi_o(x, y)] = \frac{P_o}{2\pi} \tan\theta_d \cdot \Delta\phi(x, y) \tag{1}$$

where P_o is the period of sinusoidal fringes pattern, θ_d is the angle between the axis of detection and reference plane, $\phi_r(x, y)$ is the phase value at coordinates (x, y) on the reference plane, $\phi_o(x, y)$ is the phase value at coordinates (x, y) in the presence of object, and $\Delta\phi(x, y)$ is the phase difference between $\phi_r(x, y)$ and $\phi_o(x, y)$.

Because the optical setup parameters P_o and θ_d are fixed throughout the measuring process, Eq. (1) can be simplified as

$$h(x, y) = k \cdot \Delta\phi(x, y) \tag{2}$$

where $k = \frac{P_o}{2\pi} \tan\theta_d$ is a constant for a given system setup, and can be acquired with a simple system calibration procedure described in subsection 3.2. Calculation of the surface height $h(x, y)$ is now reduced to finding the phase difference $\Delta\phi(x, y)$ at each coordinate (x, y) on the projection plane.

2.2 Extracting phase from intensity images

The intensity image $I(x, y)$ of the projected sinusoidal fringe pattern can be expressed as

$$I(x, y) = I_b(x, y) + I_m(x, y)\cos\phi(x, y) \tag{3}$$

where $I_b(x, y)$ is the background intensity, $I_m(x, y)$ is the fringe modulation, and $\phi(x, y)$ is the phase distribution at coordinates (x, y).

$I(x, y)$ in Eq. (3) is the known intensity image of the projected sinusoidal fringe pattern obtained from the CCD camera. $I_b(x, y)$, $I_m(x, y)$ and $\phi(x, y)$ are unknown in Eq. (3) and still need to be solved. To extract the phase $\phi(x, y)$, at least three different intensity images of the projected sinusoidal fringes patterns are required.

In this study, we choose $\pi/2$ as the phase shifting increment and adopt a four-step method to generate four different fringe patterns, i.e., we sequentially shift the sinusoidal fringe pattern by the phases of 0, $\pi/2$, π, and $3\pi/2$. Let $I_1(x, y)$,

$I_2(x,y)$, $I_3(x,y)$, and $I_4(x,y)$ correspond to the intensity images from phases 0, $\pi/2$, π, and $3\pi/2$, respectively. The intensity images of the projected sinusoidal fringe patterns can be formulated as

$$I_1(x,y) = I_b(x,y) + I_m(x,y)\cos[\phi(x,y)+0] = I_b(x,y) + I_m(x,y)\cdot\cos\phi(x,y)$$

$$I_2(x,y) = I_b(x,y) + I_m(x,y)\cos[\phi(x,y)+\frac{\pi}{2}] = I_b(x,y) - I_m(x,y)\sin\phi(x,y)$$

$$I_3(x,y) = I_b(x,y) + I_m(x,y)\cos[\phi(x,y)+\pi] = I_b(x,y) - I_m(x,y)\cdot\cos\phi(x,y)$$

$$I_4(x,y) = I_b(x,y) + I_m(x,y)\cos[\phi(x,y)+\frac{3\pi}{2}] = I_b(x,y) + I_m(x,y)\sin\phi(x,y)$$

By solving the four equations above, the phase distribution $\phi(x,y)$ at coordinates (x,y) can be computed as

$$\phi(x,y) = \tan^{-1}\left[\frac{I_4 - I_2}{I_1 - I_3}\right] \tag{4}$$

The reason that we adopt a four-step method, instead of a three-step method, is that zero values at the denominator in Eq. (4) can be eliminated.

The phase $\phi(x,y)$ calculated from Eq. (4), which is between $-\pi/2$ and $\pi/2$, is not the actual phase value and still cannot be used to evaluate the surface height. With the so-called modulo 2π correction [22], the calculated phase is first made to extend the range from 0 to 2π. Then the 2π discontinuities of modulo 2π phase data can be removed by adding 2π to the adjoining data according to the phase variation. The phase distributions on the reference plane and on the object, i.e., $\phi_r(x,y)$ and $\phi_o(x,y)$, can be obtained according to the forgoing phase unwrapped process. Once the phases that modulate the sinusoidal fringes on the object and on the reference plane are acquired respectively, the phase difference $\Delta\phi(x,y)$ is obtained.

Then the 3D reconstruction can be derived from Eq. (2).

3. The LCD-based 3D surface profiling system

3.1 System layout

Figure 2 shows the configuration of the proposed system. The projection unit is composed of a cool light source, the convex lens 1 and the LCD panel. We adopt the cool light source in the system so that the transparency of the LCD panel will not be affected by temperature variation [25]. The cool light source with a power range of 0-150 W and the convex lens 1 with a focal length of 50 *mm* are employed to supply the collimated white light of normal temperature. The chosen LCD panel with a resolution of 800×600 pixels has an active area of 27 × 20 mm^2. This panel is connected to a personal computer, and can be directly controlled by software to generate transparent sinusoidal gratings through the LCD control interface.

The convex lens 2 with a focal length of 50 *mm* is used to focus the images of the projected sinusoidal fringe patterns. A precision translation stage with a resolution of 0.005 *mm* is used to hold the rigid flat plate (used as the reference plane) and to place the object under inspection. The convex lens 1, the LCD panel, the convex lens 2 and the precision translation stage are all held by optical holders and fixed on a linear optical bench 50 *cm* in length. The optical setup is designed to obtain normal projection onto the reference plane.

A black and white CCD camera is implemented to capture the projected fringe patterns. The collocated lens is 50 mm, $F/1.8$. The CCD camera captures the

intensity images from a detection angle of 20 degrees. The effective size of a captured image is 640×480 pixels wide with 8-bit gray levels.

3.2 Phase shifting and adaptive projection

The sinusoidal fringe patterns can be software-generated and displayed on the LCD panel. Figure 3 shows an example of the computer-generated sinusoidal fringe pattern in this study. The sinusoidal fringe lines is perpendicular to the x-axis and its intensity distribution varies according to

$$I_n = 1 + \cos[\frac{2\pi}{P} x + \delta(t)] \tag{5}$$

where I_n is the normalized intensity, P is the fringe period, and $\delta(t)$ is the phase step.

The required sinusoidal fringe pattern is acquired by illuminating the LCD panel with the white light source and projecting it to the image plane. Shifting the computer-generated fringe pattern with the $\pi/2$ phase increment is equivalent to shifting the pattern with one fourth of the fringe period. In this study, the fringe period is measured with pixels. The required four phase-shifted sinusoidal fringe patterns with $\pi/2$ phase increment are acquired by digitally shifting the fringe pattern with the mapping fringe periods. Therefore, there are no vibrations caused by mechanical movement during the phase shifting process.

The proposed system can provide adaptive projection; that is, sinusoidal fringe patterns displayed on the LCD panel can be changed easily with different fringe

periods, phase-variation directions and grating patterns. As seen in Figure 4, the fringe period can be adjusted by changing the P value in Eq. (5). The phase-variation direction is adjusted by rotating the computer-generated sinusoidal fringe pattern with counterclockwise θ. For example, the sinusoidal fringe lines are perpendicular to the y-axis when θ is 90°. The grating pattern can be changed with shape masking. These adjustments are all done by software setting and are instantly reflected to the projected sinusoidal fringe pattern on the image plane. The adaptive projection is very useful for measuring 3D surface profiling of various electronic components on PCBs because these components generally have different sizes, topographies and reflections.

3.3 System calibration and procedure

Before proceeding to the inspection procedure for 3D object reconstruction, the k constant value in Eq. (2) must be predetermined. It can be seen from Eq. (2) that the k value can be derived from the known surface height divided by the corresponding phase difference. A simple calibration procedure based on a uniform measurement scale [26] is used to obtain the k value with a known surface height and the corresponding phase difference. The calibration procedure has the advantage that the aberrations of the optical lens and the position of the CCD camera do not have to be known and have no influence on the measurement accuracy.

The phase distribution on the flat plate is determined by the proposed system first. Then the precision translation stage that holds the flat plate is finely tuned along the z direction with a known distance Δd (as the constant surface height h). Finally, the phase distribution on the flat plate after the movement Δd is determined again by the proposed system. Following the calibration procedure described above, the

phase change $\Delta\phi$ due to a translation of the flat plate by a known distance Δd is measured using Eq. (4). Thus, the *k* value is obtained as

$$k = \frac{\Delta d}{\Delta \phi} \tag{6}$$

Once the *k* constant value is acquired, the inspection procedure of the proposed system proceeds as follows.

Step 1. Generate a fringes pattern: The sinusoidal fringe pattern is generated first using Eq. (5) displayed on the LCD panel.

Step 2. Project sinusoidal fringes: Illuminate the LCD panel with the collimated white light. The sinusoidal fringes pattern image is focused and projected onto the rigid flat plate (the reference plane).

Step 3. Shift phases: The computer-generated sinusoidal fringe pattern that displays on the LCD panel is digitally shifted in four phase steps 0, $\pi/2$, π, and $3\pi/2$.

Step 4. Generate the reference phase: The intensity images projected on the rigid flat plate are sequentially captured by the CCD camera and computed using Eq. (4) to obtain the phase values $\phi_r(x, y)$ on the reference plane.

Step 5. Generate the object phase: Place the object to be inspected on the precision translation stage and repeat Steps 3 and 4 to obtain the phase values $\phi_o(x, y)$ in the presence of the object.

Step 6. Construct a surface profile: The phase difference $\Delta\phi(x, y)$ of each coordinate (x, y) is calculated. The surface height $h(x, y)$ of the object under inspection is acquired with Eq. (2), and the 3D surface profile of the object is obtained.

4. Experimental Results

In this experiment, the test samples of standard 1 *mm*-gauge block, coin, and solder joints and SMT components on PCBs are used to evaluate the efficacy of the proposed method. All these samples are inspected by the procedure described in section 3.3. We first measure the step height of a standard 1mm gauge block of grade 0 to analyze the measuring accuracy of the proposed system. Figures 5(a)-(c) show the original image, the deformed sinusoidal fringes image, and the 3D reconstructed surface profile of the gauge block. The resulting mean step height of the projected area is 1.03 mm and the standard deviation is 0.04 mm.

Figures 6(a)-(d) show the original image, the deformed sinusoidal fringes image, the range image as an intensity function (the brightness is proportional to the height), and the 3D surface profile of a coin with a diameter of 25 mm. Although the test coin presents a complicated, metallic surface, its 3D surface profile is well reconstructed by the proposed system. Figures 7(a)-(c) show the original image, deformed fringes image and 3D surface profile of a solder joint on the PCB. Figures 8(a)-(b) show the original image and 3D surface profile of SMT components on a PCB. These components are all well reconstructed, and well separated from their complicated backgrounds of substrates.

In proceeding with these experiments, a few conditions must be noted. The adequacy of the fringe contrast must be considered first because it determines the quality of the intensity data and then the measuring precision of the surface height. Fringe contrast $\gamma(x, y)$ is the ratio function of $I_m(x, y) / I_b(x, y)$ and can be computed as

$$\gamma(x,y) = \frac{2[(I_4 - I_2)^2 + (I_1 - I_3)^2]^{1/2}}{(I_1 + I_2 + I_3 + I_4)} \tag{5}$$

where I_1, I_2, I_3, and I_4 are those defined in Eq. (4). Intensity data quality is poor when the fringe contrast is close to zero. Contrarily, a good intensity image is obtained when the fringe contrast is approximate to 1. If the fringe contrast is too low, the 3D surface profile of the object under inspection will not be properly reconstructed. In the proposed system, the fringe contrast can be improved by adjusting the output power of the cool light source and the diaphragm of the lens. Second, overexposure must be avoided because the phase value $\phi(x,y)$ associated with the surface height cannot be correctly acquired in an overexposed region. Finally, the detection angle θ_d should be less than 30°. An increment in the detection angle will induce shadow areas and generate unbalanced intensity distribution on the sensed images. Noises of 3D surface profile will be increased, which will result in increasing noise in the reconstructed profile.

It can be seen from Eq. (4) that the detected phase value is tightly related to the gray level of intensity. It indicates that the use of a higher gray-level spectrum (such as 10-bit gray levels) and spatial resolution of digitization hardware (such as 1K×1K image systems) will induce the higher measuring resolution of surface profiling. In addition, adopting a higher pixel resolution LCD panel will also generate a finer fringe period with adequate fringe contrast. A small phase change can be effectively measured with a finer fringe period and, therefore, the measuring resolution of the proposed system can be further improved.

With full-field projection and inspection, the measurement speed of the proposed

system is fast. The processing time of the 3D surface profiling for an image of 640×480 pixels wide is less than 4 seconds using a Pentium Ⅲ 500-MHz microcomputer.

4. Conclusions

In this paper, a full-field 3D surface profiling system with cost-effective equipment is presented. The proposed system is based on the projected sinusoidal fringes with phase shifting technique. A software-controlled LCD panel has been successfully used to generate sinusoidal fringe grating and achieve vibration-free phase shifting. Even though the proposed system is composed of low cost equipment, experiments have shown that the measurement process is very efficient and effective in 3D inspection of small metallic objects. The proposed system can also provide adaptive projection to accommodate the various sizes, topographies and reflections of different electronic components.

Experiments reveal that adequate projected fringe contrast is required and overexposure of images should be avoided as much as possible. The system resolution can be improved considerably by adopting a higher resolution LCD panel, image grabber and CCD. A flexible and cost-effective application of 3D inspection can be realized with the proposed technique.

References

1. D. Poussant and D. Laurendeau, “3-D sensing for industrial computer vision,” in *Advances in Machine Vision*, J. L. C. Sanz, (ed.) New York: Springer-Verlay, 1989.
2. N. Stein and H. Frohn, “Laser light stripe measurements assure correct piston assembly,” *Proceedings of SPIE*, 1989, 302-307, June. 24-25, Bellingham, WA, USA, 1993.
3. D. J. Svetkoff, D. B. Kilgus and R. C. Boman, “3D line-scan imaging with orthogonal symmetry,” *Proceedings of SPIE*, 2599, 117-188, Oct. 23-25, 1995.
4. S. B. Marapane and M. M. Trivedi, “Region-based stereo analysis for robotic applications,” *IEEE Trans. Systems, Man and Cybernetics*, 19,1447-1464, 1989.
5. T. J. Wang and T.W. Sze, “The image moment method for the limited range CT image reconstruction and pattern recognition,” *Pattern Recognition*, 34, 2145-2154, 2001.
6. M. L. Smith, G. Smith and T. Hill, “Gradient space analysis of surface defects using a photometric stereo derived bump map,” *Image and Vision Computing*, 17, 321-332, 1999.
7. N. Katafuchi, M. Sano, S. Ohara and M. Okudaira, “A method for inspecting industrial parts surfaces based on an optics model,” *Machine Vision and Applications*, 12, 170-176, 2000.
8. L. D. Stefano and F. Boland, “ Solder-paste inspection by structured light methods based on phase measurement,” *Proceedings of SPIE*, 2899, 702-713, Nov. 6-7, Bellingham, WA, USA, 1996.
9. J. L. Horijon, W. D. Amstel, F. C. Couweleer and W. C. Ligthart, “Optical system of an industrial 3D laser scanner for solder paste inspection,” *Proceedings of SPIE*, 2599, 162-170, Oct. 23-25, Bellingham, WA, USA, 1995.
10. E. H. Rideout, “Lowering test costs with 3-D solder-joint inspection,” *Test & Measurement World*, 10, 744-1657, 1990.
11. Y. K. Ryu and H. S. Cho, “New optical measuring system for solder joint inspection,” *Optics and Lasers in Engineering*, 26, 487-514, 1997.
12. H. Tsukahara, Y. Nishiyama, F. Takahashi, T. Fuse, M. Ando and T. Nishino, “High-speed 3D inspection system for solder bumps,” *Proceedings of SPIE*, 2597, 168-177, Oct. 23-25, Bellingham, WA, USA, 1995.

13. P. Kim, and S. Rhee, “Three-dimensional inspection of ball grid array using laser vision system,” *IEEE Transactions on Electronics Packaging Manufacturing*, **22**, 151-155, 1999.

14. Anon, “Microfocus X-rays for BGA/flip chip inspection,” *European Semiconductor Design Production Assembly*, 21, S61-S62, 1999.

15. S. Rooks and T. Sack, “X-ray inspection of flip chip attach using digital tomsynthesis,” *Circuit World*, 21, 51-55, 1995.

16. C. Neubauer, S. Schroepfer and R. Hanke, “X-ray inspection of solder joints by planar computer tomography,” *Proceedings of the IEEE/CPMT Intl. Electronics Manufacturing Technology Symposium*, 60-64, Sept. 12-14, 1994.

17. A. R. Kalukin, and V. Sankaran, ”Three-dimensional visualization of multilayered assemblies using X-ray laminography,” *IEEE Transactions on Components, Packaging, and Manufacturing Technology*, Part A 43, 361-666, 1997.

18. Y. Matsuyama, T. Honda, H. Yamamura, H. Sasazawa, M. Nomoto, T. Ninomiya, A. Schick, L. Listl, P. Kollensperger, D. Spriegel, P. Mengel and R. Schneider, “Automated solder joint inspection system using optical 3-D image detection,” *Proceedings 3rd IEEE Workshop on Applications of Computer Vision*, 116-122, 1996.

19. M. Noguchi and S.K. Nayar, “Microscopic shape from focus using active illumination,” *Proceedings of the 12th IAPR International Conference on Pattern Recognition*, 1, 147-152, 1994.

20. K. J. Gasvik and M. E. Fourney, “Projection moiré using digital video processing: a technique for improving the accuracy and sensitivity,” *Journal of Applied Mechanics, Transactions of the ASME*, 53, 652-656, 1986.

21. M. Aalioua and Hsin-Chu Lin, “Optical sensing techniques for 3-D machine vision,” *Proceedings of SPIE*, 665, 150-161, 1986.

22. J. E. Greivenkamp and J. H. Bruning, “Phase shifting interferometry,” in *Optical Shop Testing*, D. Malacara (ed.), Wiley, New York, 1992.

23. B. V. Dorrio and J. L. Fernandez, “Phase-evaluation methods in whole-field optical measurement techniques,” *Measurement Science*, 10, 33-55, 1999.

24. V. Srinivasan, H. C. Liu and M. Halioua, “Automated phase-measuring profilometry: a phase mapping approach,” *Applied Optics*, 24, 185-188, 1985.

25. F. Docchio, G. Sansoni and N. Viviani, “Light-induced transmission changes in liquid crystal displays for adaptive pattern projection,” *IEEE Trans. Instrument*

Measurement, 41, 629-632, 1992.

26. A. Asundi and W. Zhou, “Unified calibration technique and its applications in optical triangular profilometry,” *Applied Optics*, 38, 3556-3561, 1999.

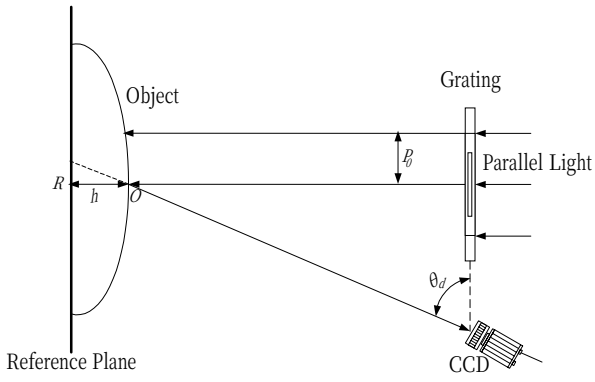

Figure 1. Optical geometry of the projected fringes method.

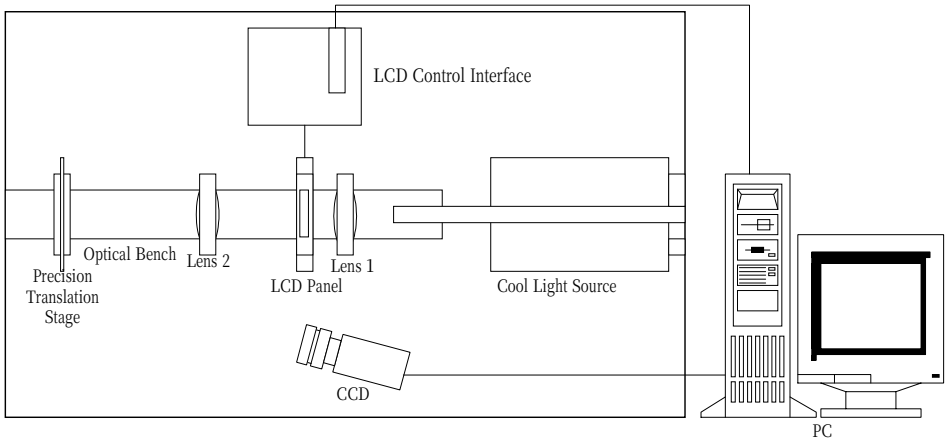

Figure 2. Configuration of the proposed 3D surface profiling system.

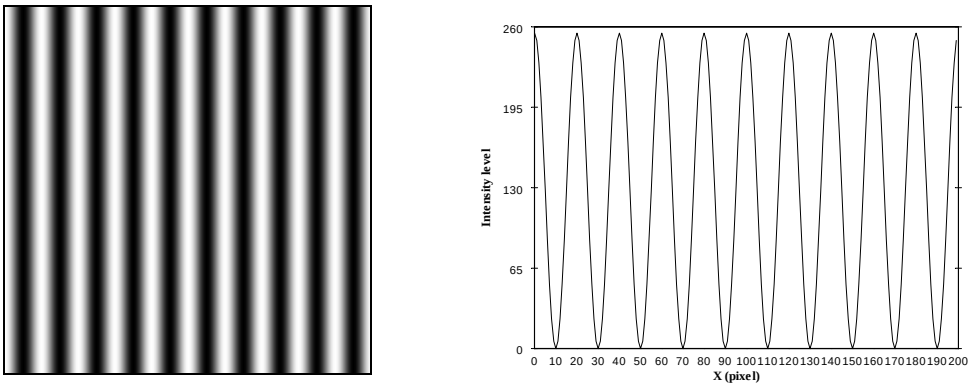

(a) (b)

Figure 3. Example of the computer-generated sinusoidal fringe pattern.

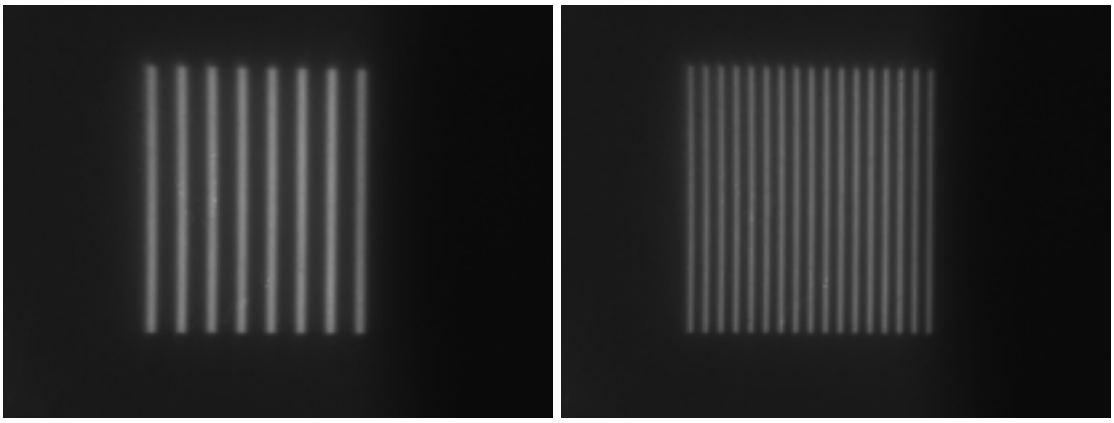

(a) The projected sinusoidal fringe pattern on the flat plane with different fringe periods.

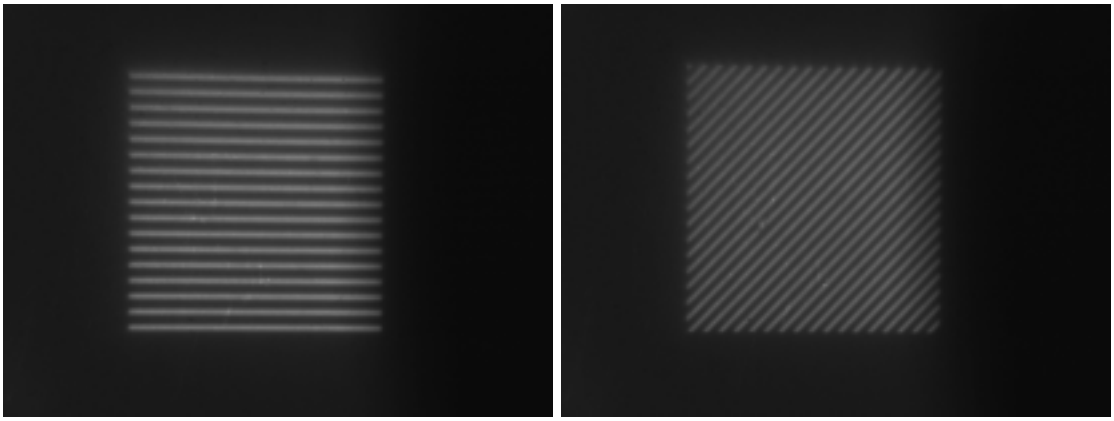

(b) The projected sinusoidal fringe pattern on the flat plane with different phase-variation directions.

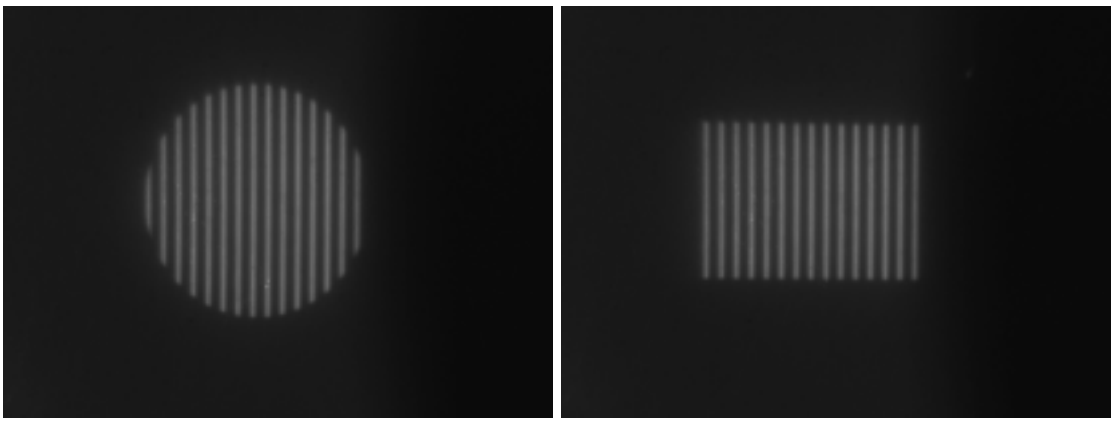

(c) The projected sinusoidal fringe pattern on the flat plane with different grating patterns.

Figure 4. The adaptive projection of the proposed system.

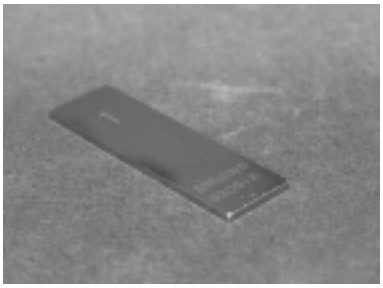

(a) The 1mm gauge block.

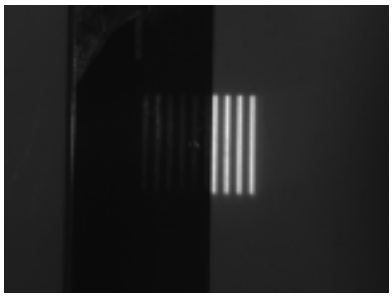

(b) The deformed sinusoidal fringes image of the 1mm gauge block.

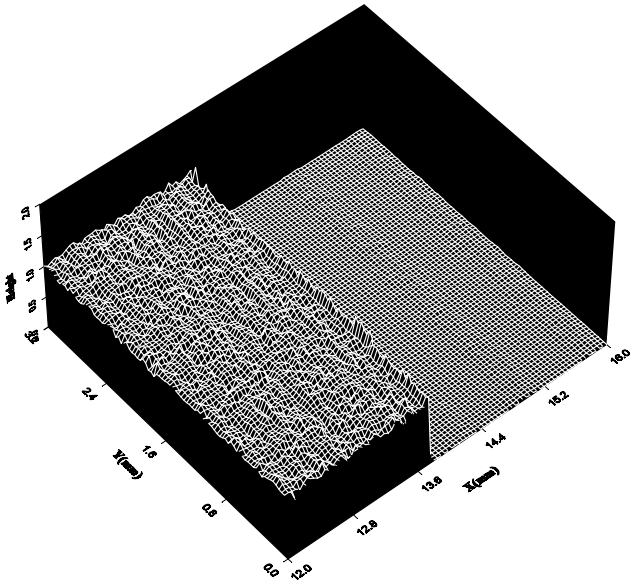

(c) The 3D surface profile of the 1mm gauge block.

Figure 5. The original image, deformed fringes image and 3D surface profile of a standard 1mm gauge block.

(a) The test coin.

(b) The deformed sinusoidal fringes image of the test coin.

(c) The range image as an intensity function, where the brightness is proportional to the height.

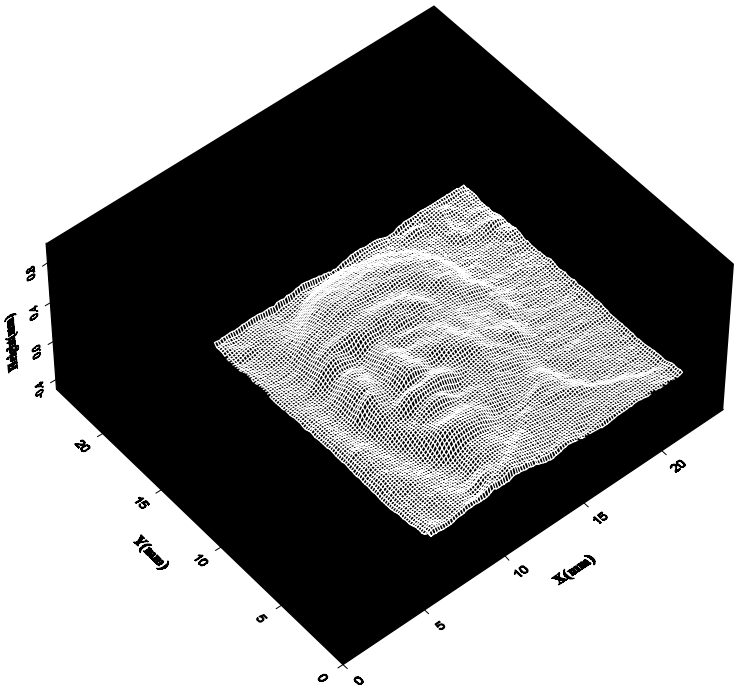

(d) The 3D surface profile of the test coin.

Figure 6. The original image, deformed fringes image, range image as an intensity function, and 3D surface profile of a test coin.

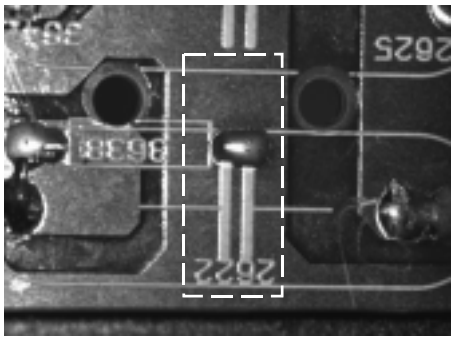

(a) A solder joint on the PCB.

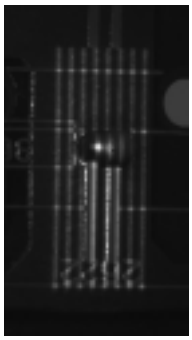

(b) The deformed sinusoidal fringes image of the solder joint on the PCB.

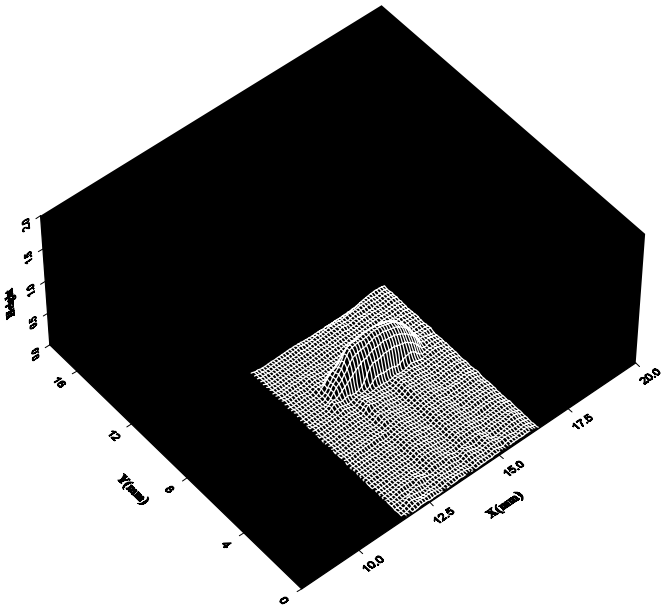

(c) The 3D surface profile of the solder joint on the PCB.

Figure 7. The original image, deformed fringes image and 3D surface profile of the solder joint on the PCB.

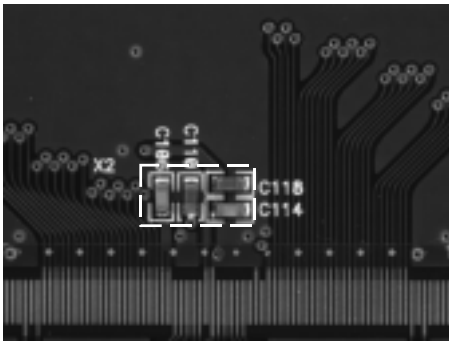

(a) SMT components on a PCB.

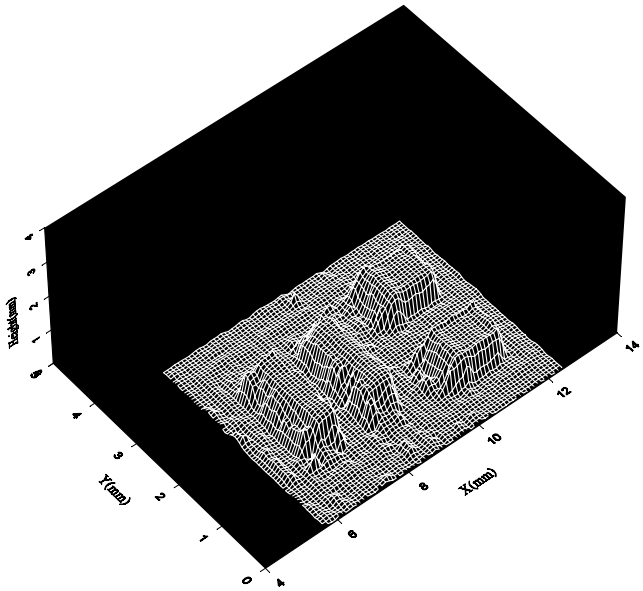

(b) The 3D surface profile of SMT components on a PCB.

Fig. 8. The original image and 3D surface profile of SMT components on a PCB.